UC Berkeley

UC Berkeley Previously Published Works

Title

An in situ ambient and cryogenic transmission electron microscopy study of the effects of temperature on dislocation behavior in CrCoNi-based high-entropy alloys with low stacking-fault energy

Permalink

https://escholarship.org/uc/item/3qn9t1f8

Journal

Applied Physics Letters, 119(26)

ISSN

0003-6951

Authors

Fang, Yan
Chen, Yujie
Chen, Bing
et al.

Publication Date

2021-12-27

DOI

10.1063/5.0069086

Peer reviewed

eScholarship.org Powered by the California Digital Library
University of California

Applied Physics Letters

An *in situ* ambient and cryogenic transmission electron microscopy study of the effects of temperature on dislocation behavior in CrCoNi-based high-entropy alloys with low stacking-fault energy

Cite as: Appl. Phys. Lett. **119**, 261903 (2021); https://doi.org/10.1063/5.0069086
Submitted: 29 August 2021 • Accepted: 29 November 2021 • Published Online: 27 December 2021

Yan Fang, Yujie Chen, Bing Chen, et al.

COLLECTIONS

Paper published as part of the special topic on Metastable High Entropy Alloys

This paper was selected as an Editor's Pick

View Online Export Citation CrossMark

ARTICLES YOU MAY BE INTERESTED IN

Effect of Al addition on the microstructures and deformation behaviors of non-equiatomic FeMnCoCr metastable high entropy alloys
Applied Physics Letters **119**, 261902 (2021); https://doi.org/10.1063/5.0069518

Tuning mechanical metastability in FeMnCo medium entropy alloys and a peek into deformable hexagonal close-packed martensite
Applied Physics Letters **119**, 261905 (2021); https://doi.org/10.1063/5.0079981

Opportunities for energy level tuning at inorganic/organic semiconductor interfaces
Applied Physics Letters **119**, 260501 (2021); https://doi.org/10.1063/5.0074963

Webinar
Interfaces: how they make or break a nanodevice
March 29th – Register now
Zurich Instruments

© 2021 Author(s).

Applied Physics Letters ARTICLE scitation.org/journal/apl

An *in situ* ambient and cryogenic transmission electron microscopy study of the effects of temperature on dislocation behavior in CrCoNi-based high-entropy alloys with low stacking-fault energy

Cite as: Appl. Phys. Lett. **119**, 261903 (2021); doi: 10.1063/5.0069086
Submitted: 29 August 2021 · Accepted: 29 November 2021 ·
Published Online: 27 December 2021

View Online Export Citation CrossMark

Yan Fang,[1] Yujie Chen,[1] Bing Chen,[2] Suzhi Li,[2] Bernd Gludovatz,[3] Eun Soo Park,[4] Guan Sheng,[5] Robert O. Ritchie,[6,7,a)] and Qian Yu[1,a)]

AFFILIATIONS

[1]Center of Electron Microscopy and State Key Laboratory of Silicon Materials, School of Materials Science and Engineering, Zhejiang University, Hangzhou 310027, China
[2]State Key Laboratory for Mechanical Behavior of Materials, Xi'an Jiaotong University, Xi'an 710049, China
[3]School of Mechanical and Manufacturing Engineering, University of New South Wales (UNSW Sydney), Sydney, NSW 2052, Australia
[4]Department of Materials Science and Engineering, Research Institute of Advanced Materials & Institute of Engineering Research, Seoul National University, Seoul 08826, South Korea
[5]Center for Electron Microscopy, State Key Laboratory Breeding Base of Green Chemistry Synthesis Technology and College of Chemical Engineering, Zhejiang University of Technology, Hangzhou 310014, China
[6]Materials Sciences Division, Lawrence Berkeley National Laboratory, Berkeley, California 94720, USA
[7]Department of Materials Science & Engineering, University of California, Berkeley, California 94720, USA

Note: This paper is part of the APL Special Collection on Metastable High Entropy Alloys.
[a)]**Authors to whom correspondence should be addressed:** roritchie@lbl.gov and yu_qian@zju.edu.cn

ABSTRACT

Temperature is known to affect deformation mechanisms in metallic alloys. As temperature decreases, the stacking-fault energy in many face-centered cubic (*fcc*) alloys decreases, resulting in a change of deformation mode from dislocation slip to deformation twinning. Such an impact of temperature can be more complex in compositionally heterogeneous microstructures that exhibit, for example, local concentration fluctuation such as that in multi-principal element alloys. In this work, we compare the dislocation behavior and mechanical properties of a *fcc* $Cr_{20}Mn_{10}Fe_{30}Co_{30}Ni_{10}$ high-entropy alloy at ambient and liquid-nitrogen temperatures. We find that a network of stacking faults is formed by uniformly extended dislocations at ambient temperatures with low stacking-fault energy, whereas at lower temperatures, uneven dissociation of dislocations becomes significant, which results in severe dislocation pile-ups together with their pronounced entanglement. Our findings indicate that as the stacking-fault energy decreases with decreasing temperature, the heterogeneity of the distribution of elements becomes more dominant in tuning the local variation of lattice resistance. As a result, the change in dislocation behavior at low temperatures strongly affects microstructural evolution and consequently leads to significantly more pronounced work hardening.

© 2021 Author(s). All article content, except where otherwise noted, is licensed under a Creative Commons Attribution (CC BY) license (http://creativecommons.org/licenses/by/4.0/). https://doi.org/10.1063/5.0069086

Multiple principal element alloys, commonly referred to as high-entropy alloys (HEAs), have been the subject of great interest as of late due to their excellent mechanical properties. This is especially true for the face-centered cubic (*fcc*) CrCoNi-based, single-phase, solid-solution alloys because of their exceptional combinations of strength, ductility, and toughness, properties that are further enhanced at low temperatures.[1–3] In general, for *fcc* alloys at ambient to cryogenic temperatures, the mechanical properties of metallic alloys are determined

© Author(s) 2021

microscopically by the formation and migration of extended defects such as dislocations and twins.[4–6] Lower homologous temperatures make the nucleation and movement of defects more difficult due to deficient thermal activation, which results in increasing strength. Opposing this is the fact that the stacking-fault energy (SFE), a key property controlling the prevailing deformation mechanisms and, hence, mechanical performance, is also strongly temperature dependent.[7,8] These factors compete such that the combined effect determines the defect behavior and the microstructural evolution at low temperatures.

For the CrMnFeCoNi system high-entropy alloys, in general, previous studies have reported that martensitic transformation occurs when the SFE is less than ∼20 mJ/m^2, twin deformation prevails when the SFE is between 20 and 40 mJ/m^2, and above ∼40 mJ/m^2, the slip of full dislocations becomes the dominant deformation mechanism.[4,9,10] For the equiatomic CrMnFeCoNi alloy, partial and full dislocation motion dominates deformation at ambient temperatures, whereas with decreasing temperature, the elevation in strength activates deformation twinning. Until recently, such CrCoNi-based HEAs have been regarded as multi-component alloys with low or relatively low SFE, which are random solid solutions.[1,11] However, since heterogeneity in chemical distributions, such as concentration fluctuation, has been identified in multiple-principal element alloys both theoretically[12,13] and experimentally,[14–16] a non-trivial interplay of local chemical fluctuations and SFEs should be considered, which is potentially tunable to introduce more complex deformation mechanisms in these alloys.[17–21] Such local deviations from a purely random solid solution can affect the slip behavior of individual dislocations and their interactions at different temperatures, which, in turn, influences the work-hardening behavior of these alloys. Indeed, it is the synergy of deformation mechanisms[22] that serves to promote steady and prolonged work hardening, which is the key to the excellent combinations of strength, ductility, and hence, toughness properties of many *fcc* HEAs.

Since changing the ratio of elements and substituting or adding alloying elements in HEAs can significantly vary the degree of local variations in chemical compositions,[14,23] we investigate here the effects of temperature on the dislocation structure and slip behavior and the resulting evolution of dislocation networks in a $Cr_{20}Mn_{10}Fe_{30}Co_{30}Ni_{10}$ (at%) HEA, a non-equiatomic variation of the Cantor alloy developed to promote a transformation-induced plasticity (TRIP) effect. Specifically, we performed real-time deformation experiments in the transmission electron microscope at two different temperatures, namely, ambient (293 K) and liquid-nitrogen (77 K) temperatures, to discern the salient plasticity mechanisms in terms of the resulting mechanical properties. We find that deformation in this alloy at 293 K is associated with the dissociation of dislocations into partials with the consequent creation of stacking faults. These stacking faults formed on different planes lead to the generation of parallelogram-shaped dislocation networks, which act to markedly impede dislocation motion by slip. With rising plastic strain, however, increasing interaction between dislocations results in leftover sessile segments, which further serve as continuous obstacles. Based on these deformation mechanisms at ambient temperatures, the work-hardening rate of the $Cr_{20}Mn_{10}Fe_{30}Co_{30}Ni_{10}$ HEA is quite comparable to the equiatomic Cantor alloy. At low temperatures, conversely, significant nanoscale segment detrapping (the stick-slip dislocation forward-glide)[19] is observed. Although the SFE is decreased with decreasing temperature, the influence of the heterogeneity of the element distribution may become more significant on the lattice resistance; strong local pinning, thus, appeared that increased the difficulty of the uniform dissociation of dislocations. Such stick-slip dislocation forward-glide results in severe dislocation tangling and pile-ups. Rather than forming a metastable dislocation network similar to that at 293 K, a far more stable dislocation network is developed at 77 K, such that the alloy exhibits a significantly higher work-hardening rate than that in the Cantor alloy.

In this study, the $Cr_{20}Mn_{10}Fe_{30}Co_{30}Ni_{10}$ alloy was prepared by arc melting of pure metals (purity > 99.9%) and then drop-casting the molten alloy into a cooper mold; the resulting ingot was then recrystallized at 1073 K for 20 min. With this composition, the alloy is believed to display much stronger local chemical variations compared to that in the equiatomic Cantor alloy.[24,25]

The samples for transmission electron microscopy (TEM) imaging were first polished with SiC paper down to a thickness of ∼80 μm and punched into disks with a diameter of 3 mm. To achieve electron-transparent regions, the samples were further thinned by twin-jet polishing in a perchloric acid solution, comprising 60% methanol, 34% n-butyl alcohol, and 6% perchloric acid. *In situ* TEM samples were prepared by gluing the samples to stainless-steel substrates with narrow rectangular windows for transmission in the electron beam.

Microstructure characterization was primarily conducted by TEM and scanning TEM-high-angle annular dark-field (STEM-HAADF). *In situ* straining experiments were performed in a FEI Tecnai G2 F20 TEM operating at 200 kV, using a Gatan 671 single-tilt straining holder. An FEI Titan Chemi-STEM G2 80–200 with a spherical aberration corrector operating at 200 kV was used to acquire the HAADF images. A spherical aberration-corrected scanning transmission electron microscope operated at 300 kV was used to perform the atomic-resolution energy-dispersive x-ray spectroscopy (EDS) mapping. In order to obtain a high signal-to-noise ratio, a complete process of EDS mapping took roughly 1.5 h when the beam current was set between 25 and 30 pA.

Uniaxial tensile tests were carried out on an Instron 5967 universal testing machine (Instron, Norwood, USA) at a strain rate of 1×10^{-3} s^{-1} at ambient temperature and liquid nitrogen temperature.

The generalized stacking-fault energies in the CrMnFeCoNi system were calculated using the modified embedded atom method (MEAM) developed by Choi *et al.*[26] The simulation box was oriented as x-[110], y-[$\bar{1}$11], and z-[1$\bar{1}$2] with dimensions of $12 \times 12 \times 14$ nm^2. Periodic boundary conditions were applied along the x and z directions, with the free boundary condition applied along the y direction. To study the influence of temperature on the stacking-fault energies, the initial thermal equilibrated structure was relaxed at temperatures ranging from 77 to 300 K under the Nosé–Hoover thermostat.[27,28] All simulations were carried out using the LAMMPS code.[29]

The typical dislocation configuration in the bulk $Cr_{20}Mn_{10}Fe_{30}Co_{30}Ni_{10}$ HEA after deformation at ambient temperature is shown in Figs. 1(a)–1(c). Dislocations can be seen to be dissociated into partial dislocations with a relatively even width of separating stacking fault [Fig. 1(a)]. The dislocation lines of both the leading and trailing partials were quite straight, which is indicative of insignificant pinning of the dislocations. Additionally, dislocations from different slip planes interact leading to the construction of a dislocation network.

At higher strain (∼10%), assembled stacking-fault networks were created with dislocations tangled and pinned at the network; these

© Author(s) 2021

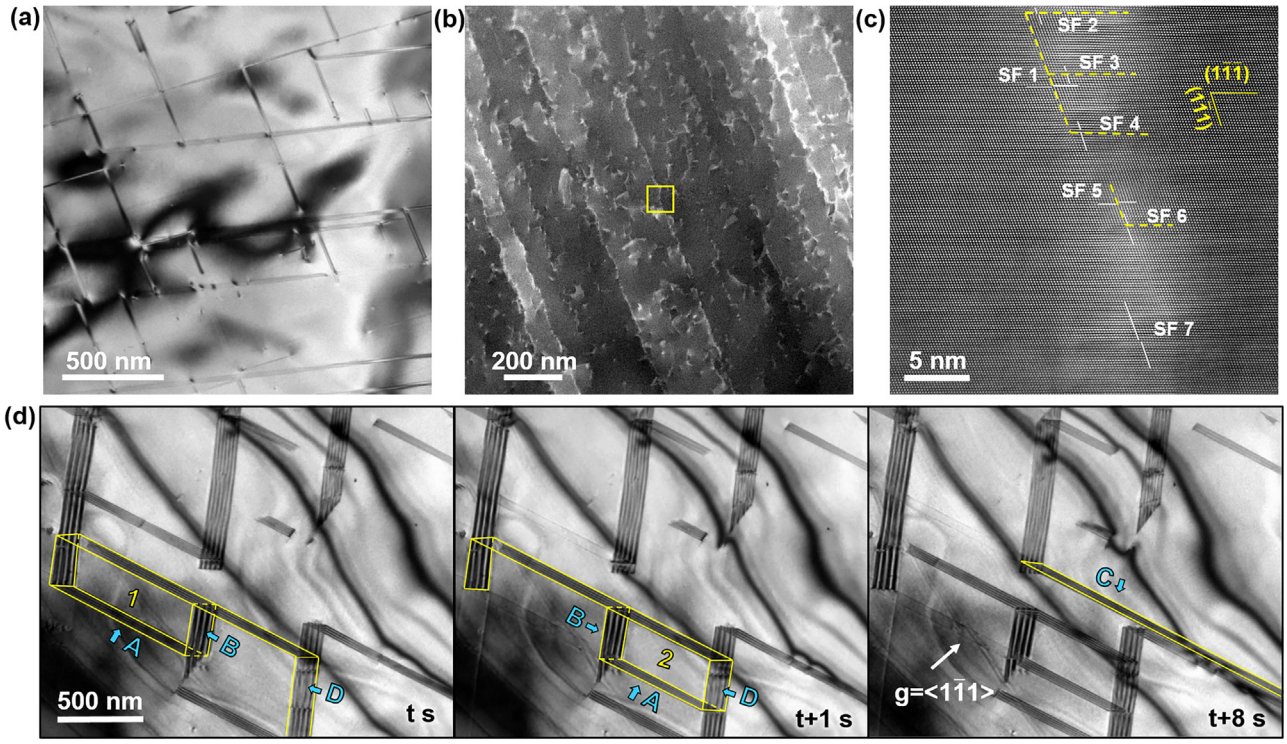

FIG. 1. TEM and STEM characterizations of the $Cr_{20}Mn_{10}Fe_{30}Co_{30}Ni_{10}$ alloy deformed at room temperature. (a) Bright-field TEM image of the stacking-fault network, (b) the HADDF-STEM image of the assembled stacking faults, (c) enlarged image of the region marked by the yellow box in (b), showing the atomic structure of the assembled dislocation. For instance, a Lomer–Cottrell lock resulting from the reaction of two partial dislocations, with stacking fault SF1 and SF2, marked by the yellow dashed lines; SF3 is hindered by SF1. Similar reactions and structures can be seen in SF4 to SF7. (d) A sequence of TEM images showing the dynamic process of the generation and subsequent evolution of a stacking-fault network. The leading partial of stacking fault A was first hindered by the stacking fault B forming a stacking-fault parallelogram 1, and then hindered by the stacking fault D forming stacking-fault parallelogram 2.

networks can be seen in the HAADF-STEM images in Figs. 1(b) and 1(c). The HAADF-STEM image in Fig. 1(c), which is the magnified image of the yellow box in Fig. 1(b), shows the real space atomic structure of one such dislocation interaction, taken along the [110] zone axis. An extremely high density of extended dislocations can be observed. Since the dislocations were activated on multiple parallel slip planes and in different slip systems, the interaction of partial dislocations at different junctions promoted the formation of these parallelogram-shaped stacking-fault networks; furthermore, nanoscale stacking-fault networks, marked by yellow-dashed lines, can also be seen. This dislocation is located on a (001) plane with a Burgers vector of $a/6[1\bar{1}0]$ after reaction of at least two stacking faults, such as SF1 and SF2, i.e., $a/2[101]$ and $a/2[0\bar{1}\bar{1}]$, respectively, on $(1\bar{1}\bar{1})$ and $(1\bar{1}1)$ planes. It is termed a Lomer-Cottrell lock,[30] serving as immobile dislocation that arrests the motion of the trailing partials. These sessile dislocations are commonly found in the $Cr_{20}Mn_{10}Fe_{30}Co_{30}Ni_{10}$ alloy at ambient temperatures and serve to stabilize the stacking-fault networks.

To examine the evolution of the stacking-fault network and its subsequent stability, we used a set-up in the TEM, described previously in Ref. 23, that allows for real-time observation of the dynamic activities of defects. Figure 1(d) established a series of snapshots captured from supplementary material, Video 1, showing the typical evolution of stacking-fault networks. It was observed that in the early stage of deformation, the movement of partial dislocations is easy. According to our observations over a wide range of strains (>10%), partial dislocation activity from different slip systems results in frequent dislocation interactions, creating sessile dislocation junctions. As shown in Fig. 1(d), the sessile dislocation junctions act to specifically promote the formation of the stacking-fault networks, as marked by the blue arrows. These networks, however, are changeable due to the variation in the mobility of the partial dislocations under different applied stresses. For instance, the leading partial of stacking fault A was initially hindered by stacking fault B, forming a stacking-fault parallelogram 1, profiled by the yellow lines. As the applied stress increased, the trailing partial of stacking fault A caught up and stacking-fault A disappeared. The leading partial of stacking fault A further overcame the impediment of stacking fault B but stopped at stacking fault D, temporarily forming another stacking-fault parallelogram 2. These scenarios were repeated throughout the deformed region such as at the location of stacking fault C. As the stacking-fault network further evolved, the slip of a leading partial dislocation from the opposite direction encountered stacking fault C, leading to the construction of a new stacking-fault parallelogram.

In contrast, the behavior of dislocations and the morphology of their interactions in the $Cr_{20}Mn_{10}Fe_{30}Co_{30}Ni_{10}$ HEA were quite

© Author(s) 2021

distinct for deformation at liquid nitrogen temperature. Since the stacking-fault energy of this alloy is so low, many dislocations appeared to dissociate into partials, as shown in Fig. 2. However, the details of the resulting configuration of the individual dislocation lines, in particular the degree of dissociation in each dislocation as well as the dislocation network structures that were developed, were significantly different. The average dissociation width of dislocations at cryogenic temperatures was clearly shorter than that at ambient temperature. The dissociation of dislocations was broadly observed, although a higher portion of full (undissociated) dislocations was apparent at the low temperature, as shown by the blue and yellow arrows in Fig. 2(a). Figure 2(b) is the magnified TEM image showing the typical extended dislocation in the region marked by yellow square in Fig. 2(a). The distinctly different variation of dissociation with large number of local pinning points appeared along the dislocation lines (stroked by yellow dashed lines). Consequently, the dislocations severely tangle locally under strain, as shown in Fig. 2(c). Unlike the parallelogram-shaped stacking-fault networks that are formed at room temperature, this entanglement is far more chaotic. Multiple dislocations with complex dissociation morphologies react with each other, which makes the entanglement more difficult to dismantle.

The dynamic evolution of such complex tangled dislocation structures at liquid-nitrogen temperature can be clearly observed under *in situ* cryo-TEM straining conditions, as shown in Fig. 2(d); supplementary material, Video 2 images the process of formation in real time. It is also evident that the movement of the partial dislocation is more sluggish at 77 K, indicating a considerable resistance to dislocation slip at the low temperature. Strong waviness with roughness down to nanometer scale is seen along the dislocation line as dislocation gliding (as shown in the magnified images in the top left corners). In addition, the morphology of dislocations continuously changes during dislocation slip, which is similar with our previous observations[23] in the CrCoNi-W alloy. The dislocations marked by the blue (dislocation 1) and red arrows (dislocation 2) in Fig. 2(d) were seen to dissociate unevenly and subsequently display different velocities for each of the nano-segments. For instance, dislocation 2 (marked by the red profile) shows strong waviness with the size of each segment down to the nanometer scale, indicating a strong pinning effect. As a result, with increasing applied strain, the consequent accumulation of such stick-slip dislocation forward-glide, namely, nanoscale segment detrapping, resulted in severe entanglement. Such different dislocation behavior at ambient vs cryogenic temperatures, with the resulting development of the dislocation structures and networks, undoubtedly is expected to have a significant impact on the mechanical properties of this alloy, as discussed in the following section. The engineering uniaxial stress–strain curves and the work-hardening rate for $Cr_{20}Mn_{10}Fe_{30}Co_{30}Ni_{10}$ HEA at ambient (293 K) and liquid-nitrogen (77 K) temperatures are compared to those of the equiatomic CrMnFeCoNi Cantor alloy in Figs. 3(a) and 3(b). At 293 K, the Cantor displays yield and ultimate tensile strengths of 425 and 750 MPa,

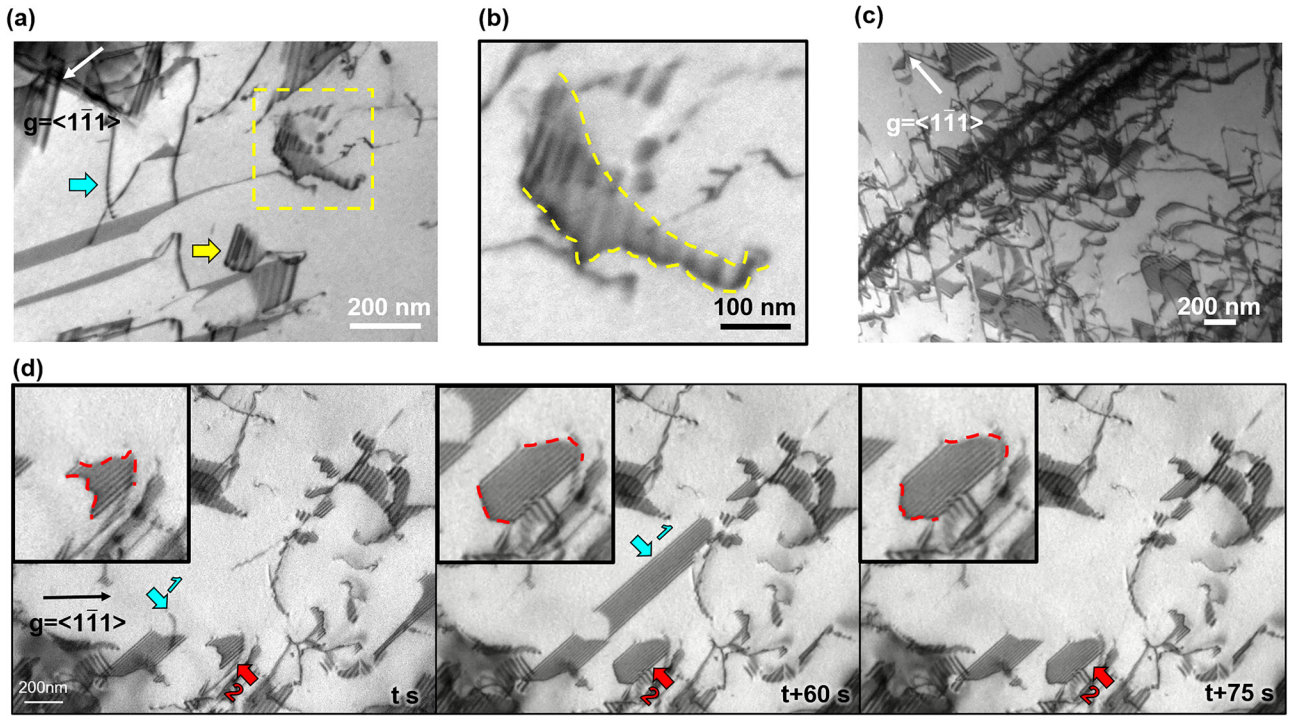

FIG. 2. TEM characterization of dislocations in $Cr_{20}Mn_{10}Fe_{30}Co_{30}Ni_{10}$ deformed at liquid nitrogen temperatures. (a) TEM image of a typical dislocation morphology. The blue and yellow arrows show the full dislocation and the extended dislocation, respectively. The typical extended dislocation in the region marked by yellow square is magnified and shown in (b). The yellow dashed lines depicted the outline of extended dislocation with large number of local pinning points. (c) TEM image showing severely tangled dislocations. (d) *In situ* TEM tensile experiment at liquid nitrogen temperature. The extended dislocation motion marked by blue (dislocation 1) and red arrows (dislocation 2) is sluggish and encounters nanoscale segment detrapping. The insets show enlarged views of dislocation 2.

© Author(s) 2021

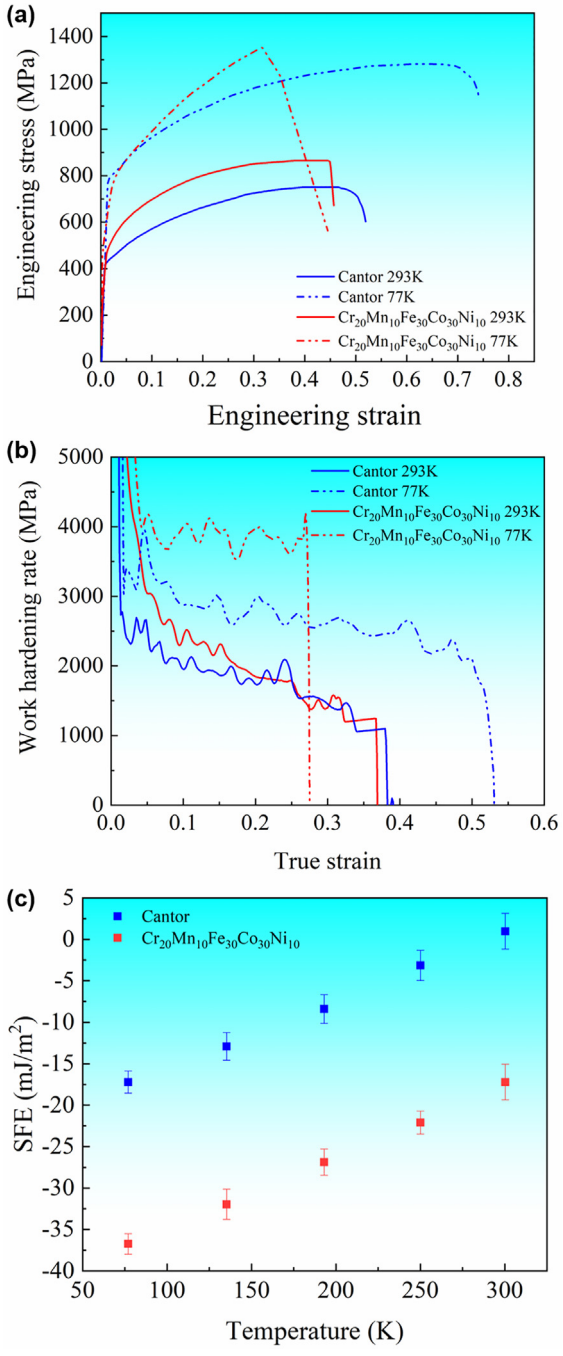

FIG. 3. Comparison of mechanical properties of the $Cr_{20}Mn_{10}Fe_{30}Co_{30}Ni_{10}$ HEA with the equiatomic CrMnFeCoNi (Cantor) alloy. (a) Measured engineering stress-strain curves of $Cr_{20}Mn_{10}Fe_{30}Co_{30}Ni_{10}$ and Cantor alloys deformed at ambient temperature and at liquid-nitrogen temperature, showing the higher tensile strength and significantly higher work hardening rate at 77 K in the $Cr_{20}Mn_{10}Fe_{30}Co_{30}Ni_{10}$ alloy. (b) Resulting strain-hardening rate derived from the stress-strain curves in (a). (c) The variation of stacking-fault energy as a function of temperature for the $Cr_{20}Mn_{10}Fe_{30}Co_{30}Ni_{10}$ and Cantor alloys, predicted by a random solid solution model.[26]

respectively, whereas the corresponding values for the $Cr_{20}Mn_{10}Fe_{30}Co_{30}Ni_{10}$ HEA are 480 and 850 MPa, indicating a slight improvement in strength for the latter alloy; both alloys exhibit tensile ductility approaching 50%. The $Cr_{20}Mn_{10}Fe_{30}Co_{30}Ni_{10}$ alloy is somewhat stronger at 77 K with respective yield and tensile strengths of 800 and 1350 MPa compared to 790 and 1270 MPa for the Cantor alloy, respectively; the ductility decreases in both alloys but is still relatively high at ~35%. More importantly, a far higher strain-hardening rate is achieved in the $Cr_{20}Mn_{10}Fe_{30}Co_{30}Ni_{10}$ alloy at low temperatures; the hardening is continuous out to a strain of ~35% and operates at a much higher stress.

In summary, the dislocation behavior and resulting dislocation networks/configurations in high-entropy alloys appear to be highly tunable as relatively small changes in composition can enact major changes in the resistance to dislocation slip. One explanation of such modifications can be associated with the heterogenous distribution of different elements in these multiple element concentrated solid solutions and the effect that this has on the variation in local composition at the nanoscale. Compared to its behavior at 293 K, the severe dislocation tangling and the complex dislocation network developed at low temperatures in $Cr_{20}Mn_{10}Fe_{30}Co_{30}Ni_{10}$ clearly result in much higher work hardening in this alloy than in the Cantor alloy at ambient and low temperatures. Since the dislocation slip is affected by bond strength, local stacking-fault energy, and lattice distortion, we used first principles calculations to study the change of generalized stacking-fault energy of the Cantor and $Cr_{20}Mn_{10}Fe_{30}Co_{30}Ni_{10}$ alloys from ambient to liquid-nitrogen temperatures. The calculation assumed that the Cantor and $Cr_{20}Mn_{10}Fe_{30}Co_{30}Ni_{10}$ alloys could be considered as random solid solutions. As shown in Fig. 3(c), while the predicted generalized stacking-fault energy of the $Cr_{20}Mn_{10}Fe_{30}Co_{30}Ni_{10}$ alloy is lower than that predicted for the Cantor alloy, the trend in both alloys is identical. However, the result demonstrates that even though the generalized stacking-fault energy is lower, the width of stacking faults in $Cr_{20}Mn_{10}Fe_{30}Co_{30}Ni_{10}$ observed at 77 K is smaller than that observed at 293 K, which is contrary to the expected behavior, that the width of the stacking fault is inversely proportional to the stacking-fault energy. Dislocations could be strongly pinned due to the large compositional variation at some local sites as the temperature is decreased to 77 K, as shown in Fig. 4(a). The observed stacking fault with a narrow width might arise from the relatively high barrier for the full dislocations to extend completely. Accordingly, even in random solid-solution CrCoNi alloys, the fluctuation in stacking-fault energy occurs over a large range (−140 to 65 mJ/m^2), while the average energy is calculated as −42.9 mJ/m^2.[31] Therefore, even though the generalized stacking-fault energy decreases as the temperature decreases, the local stacking-fault energy may still maintain a high in specific regions, leading to a wide range in its values.

We attribute these apparent anomalies to the effect of heterogeneity of the local chemical distribution in the $Cr_{20}Mn_{10}Fe_{30}Co_{30}Ni_{10}$ alloy. To verify the element distribution and reveal the corresponding relationship with dislocation behavior, we investigated the atomic-scale element distributions in $Cr_{20}Mn_{10}Fe_{30}Co_{30}Ni_{10}$ HEA by using the EDS (details are given in the Methods section). Figure 4(a) presents the atomic-resolution HAADF images and corresponding EDS maps of the $Cr_{20}Mn_{10}Fe_{30}Co_{30}Ni_{10}$ HEA with [110] zone axis. On each map for a specific element such as Cr, the brightness of an individual spot is positively correlated with the local Cr density in the

© Author(s) 2021

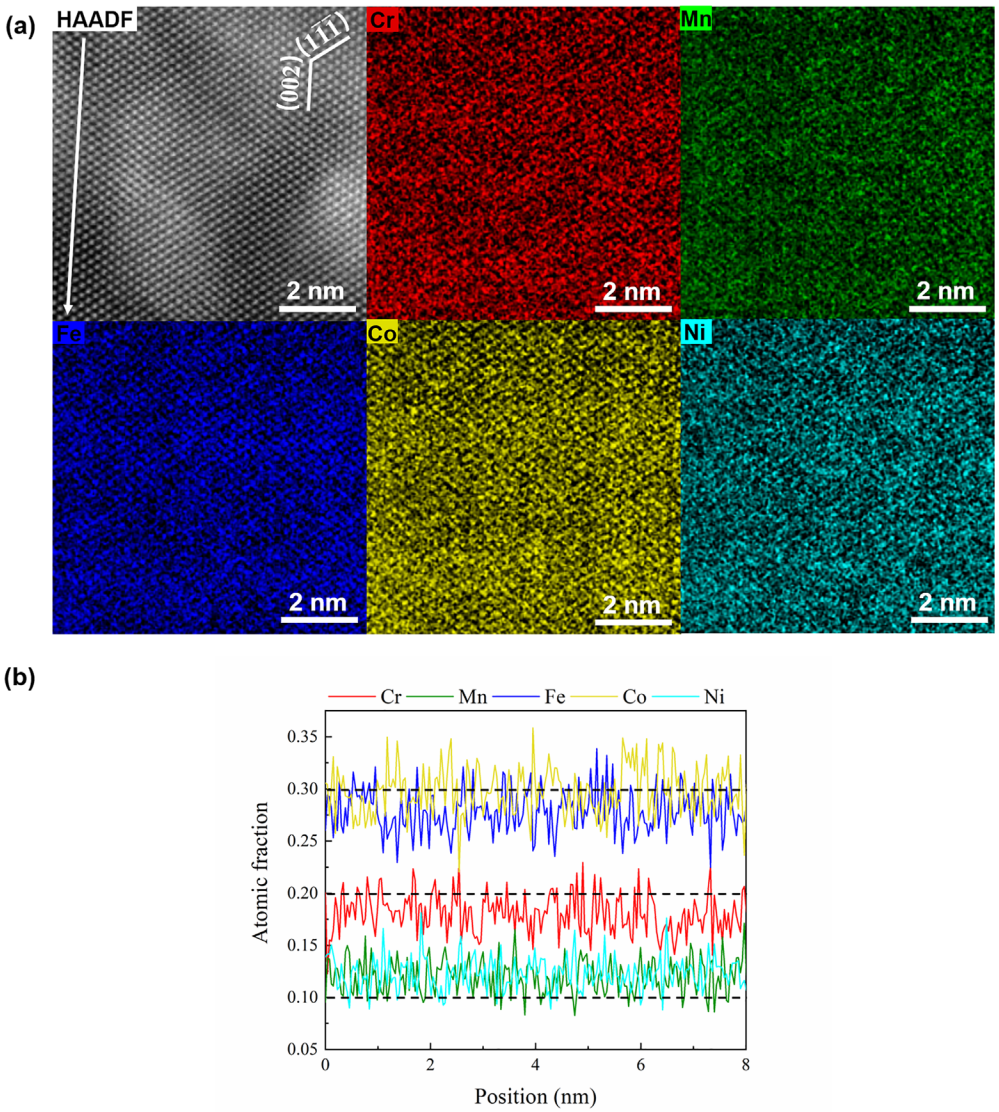

FIG. 4. Atomic-resolution EDS mapping and corresponding line profiles of the atomic fraction of individual elements in $Cr_{20}Mn_{10}Fe_{30}Co_{30}Ni_{10}$. (a) HADDF image of the atomic structure, taken in the [110] zone axis and corresponding EDS maps for individual elements. (b) Line profiles of atomic fraction of individual elements along the white line in (a). The average concentration values of all five elements deviate from the stoichiometric ratio.

atomic column along [110]. From the maps in Fig. 4(b), some random density variations can be seen for all five elements. As can be seen in the line profile in Fig. 4(b), the atomic fraction of Co, Cr, Ni, Fe, or Mn in each projected atomic column randomly fluctuates with some variation being evident. The distance between the concentration peaks and valleys of each element is at the scale of 1–3 nm. In Co, for example, the atomic fractions can reach up to ~36% and approach a minimum of about 22%; and in Mn, which accounts for only 10 at. % in the $Cr_{20}Mn_{10}Fe_{30}Co_{30}Ni_{10}$ alloy, variations between 8 and 17 at. % occur, as displayed in the line profile shown in Fig. 4(b). The concentration fluctuations of Cr, Mn, and Ni in the alloy are ~55%, ~70%, and ~80% relative to their nominal concentration, respectively. As a comparison, previous work has shown that the local elements' concentration in the Cantor alloy varies between ~15% and ~25%. Each element in the Cantor alloy has a composition fluctuation of about 50% relative to the nominal content of ~20%.[14] It should also be noted that the spatial length of heterogeneity and dislocation structure do not correspond one-to-one. The strong local pinning appeared temporarily and randomly along the dislocation lines, but the distance between each pinning point is much larger than the "period" of the fluctuation in local composition.

© Author(s) 2021

During the dislocation slip, the local chemical heterogeneity creates large numbers of pinning points that are difficult to overcome the thermal vibration of atoms, so that the dissociation of dislocations never reaches equilibrium width, which is determined by stacking-fault energy. Since the dislocation slip is strongly hindered, twinning deformation is impeded as well since it requires a continuous slip of the same partial dislocation layer by layer. As dislocations interact with regions containing some degree of chemical fluctuation, they need to encounter alternated resistance, which requires additional energy. This phenomenon becomes progressively more active as the thermal activation of the defects increases at low temperature. The results demonstrate that, distinct from traditional dilute solid-solution alloys, the temperature effect on dislocation behavior in multiple principal element alloys is likely to be strongly related to the degree of heterogeneity of their chemical distribution, coupled with the temperature-dependent variation in the thermal activation of defects; this may overwhelm the usual influence of the generalized stacking-fault energy. Such a change in dislocation behavior would consequently modify the microstructural evolution and work-hardening behavior of high-entropy alloys at varying temperatures.

See the supplementary material for (a) Movie 1: Dislocation motion in the $Cr_{20}Mn_{10}Fe_{30}Co_{30}Ni_{10}$ alloy at ambient temperature and (b) Movie 2: Dislocation motion in the $Cr_{20}Mn_{10}Fe_{30}Co_{30}Ni_{10}$ alloy at liquid-nitrogen temperature.

This work was supported by the National Natural Science Foundation of China (Grant Nos. 51671168 and 51871197), National Key Research and Development Program of China (Grant No. 2017YFA0208200), and the National 111 project (Grant No. B16042). R.O.R. was supported by the U.S. Department of Energy, Office of Science, Office of Basic Energy Sciences, Materials Sciences and Engineering Division, under Contract No. DE-AC02-05-CH11231 within the Damage-Tolerance in Structural Materials (KC-13) program at the Lawrence Berkeley National Laboratory. B.G. acknowledges support of the ARC Future Fellowship (Project No. FT190100484) and the UNSW Scientia Fellowship schemes.

AUTHOR DECLARATIONS

Conflict of Interest

The authors have no conflicts to disclose.

Author Contributions

Y.F. and Y.C. contributed equally to this work.

DATA AVAILABILITY

The data that support the findings of this study are available from the corresponding authors upon reasonable request.

REFERENCES

[1]Z. F. He, N. Jia, D. Ma, H. L. Yan, Z. M. Li, and D. Raabe, Mater. Sci. Eng. A **759**, 437 (2019).
[2]A. Gali and E. P. George, Intermetallics **39**, 74 (2013).
[3]B. Gludovatz, A. Hohenwarter, D. Catoor, E. H. Chang, E. P. George, and R. O. Ritchie, Science **345**, 1153 (2014).
[4]F. Otto, A. Dlouhý, C. Somsen, H. Bei, G. Eggeler, and E. P. George, Acta Mater. **61**, 5743 (2013).
[5]T. W. Zhang, S. G. Ma, D. Zhao, Y. C. Wu, Y. Zhang, Z. H. Wang, and J. W. Qiao, Int. J. Plast. **124**, 226 (2020).
[6]G. Laplanche, A. Kostka, C. Reinhart, J. Hunfeld, G. Eggeler, and E. P. George, Acta Mater. **128**, 292 (2017).
[7]L. Tang, K. Yan, B. Cai, Y. Wang, B. Liu, S. Kabra, M. M. Attallah, and Y. Liu, Scr. Mater. **178**, 166 (2020).
[8]S. Huang, W. Li, S. Lu, F. Tian, J. Shen, E. Holmström, and L. Vitos, Scr. Mater. **108**, 44 (2015).
[9]A. K. Chandan, S. Tripathy, B. Sen, M. Ghosh, and S. Ghosh Chowdhury, Scr. Mater. **199**, 113891 (2021).
[10]S. Allain, J.-P. Chateau, O. Bouaziz, S. Migot, and N. Guelton, Mater. Sci. Eng. A **387–389**, 158 (2004).
[11]W. Fu, K. Gan, Y. Huang, Z. Ning, J. Sun, and F. Cao, J. Alloys Compd. **872**, 159606 (2021).
[12]E. Antillon, C. Woodward, S. I. Rao, B. Akdim, and T. A. Parthasarathy, Acta Mater. **190**, 29 (2020).
[13]Y. Liu, G.-P. Zheng, and M. Li, J. Alloys Compd. **843**, 156060 (2020).
[14]Q. Ding, Y. Zhang, X. Chen, X. Fu, D. Chen, S. Chen, L. Gu, F. Wei, H. Bei, Y. Gao, M. Wen, J. Li, Z. Zhang, T. Zhu, R. O. Ritchie, and Q. Yu, Nature **574**, 223 (2019).
[15]R. Zhang, S. Zhao, J. Ding, Y. Chong, T. Jia, C. Ophus, M. Asta, R. O. Ritchie, and A. M. Minor, Nature **581**, 283 (2020).
[16]X. Chen, Q. Wang, Z. Cheng, M. Zhu, H. Zhou, P. Jiang, L. Zhou, Q. Xue, F. Yuan, J. Zhu, X. Wu, and E. Ma, Nature **592**, 712 (2021).
[17]Z.-H. Lai, Y.-H. Sun, Y.-T. Lin, J.-F. Tu, and H.-W. Yen, Acta Mater. **210**, 116814 (2021).
[18]J. Miao, C. Slone, S. Dasari, M. Ghazisaeidi, R. Banerjee, E. P. George, and M. J. Mills, Acta Mater. **210**, 116829 (2021).
[19]Q.-J. Li, H. Sheng, and E. Ma, Nat. Commun. **10**, 3563 (2019).
[20]Y. H. Zhang, Y. Zhuang, A. Hu, J. J. Kai, and C. T. Liu, Scr. Mater. **130**, 96 (2017).
[21]Y. Wu, F. Zhang, X. Yuan, H. Huang, X. Wen, Y. Wang, M. Zhang, H. Wu, X. Liu, H. Wang, S. Jiang, and Z. Lu, J. Mater. Sci. Technol. **62**, 214 (2021).
[22]Z. Zhang, M. M. Mao, J. Wang, B. Gludovatz, Z. Zhang, S. X. Mao, E. P. George, Q. Yu, and R. O. Ritchie, Nat. Commun. **6**, 10143 (2015).
[23]Y. Chen, Y. Fang, X. Fu, Y. Lu, S. Chen, H. Bei, and Q. Yu, J. Mater. Sci. Technol. **73**, 101 (2021).
[24]A. Tamm, A. Aabloo, M. Klintenberg, M. Stocks, and A. Caro, Acta Mater. **99**, 307 (2015).
[25]B. Schönfeld, C. R. Sax, J. Zemp, M. Engelke, P. Boesecke, T. Kresse, T. Boll, T. Al-Kassab, O. E. Peil, and A. V. Ruban, Phys. Rev. B **99**, 014206 (2019).
[26]W.-M. Choi, Y. H. Jo, S. S. Sohn, S. Lee, and B.-J. Lee, npj Comput. Mater. **4**, 1 (2018).
[27]S. Nosé, J. Chem. Phys. **81**, 511 (1984).
[28]W. G. Hoover, Phys. Rev. A **31**, 1695 (1985).
[29]S. Plimpton, J. Comput. Phys. **117**, 1 (1995).
[30]A. H. Cottrell, Prog. Met. Phys. **4**, 205 (1953).
[31]J. Ding, Q. Yu, M. Asta, and R. O. Ritchie, Proc. Natl. Acad. Sci. **115**, 8919 (2018).

© Author(s) 2021